02

Optoelectronic properties of highly doped Ge:Sb layers prepared by ion-beam methods

© H.A. Novikov[1], R.I. Batalov[1], I.A. Faizrakhmanov[1], V.A. Shustov[1], S.G. Simakin[2], K.N. Galkin[3], N.A. Baidakova[4]

[1] Zavoisky Physical-Technical Institute, FRC „Kazan Scientific Center of RAS“, Kazan, Russia
[2] Valiev Institute of Physics and Technology of RAS, Yaroslavl Branch, Yaroslavl, Russia
[3] Institute of Automation and Control Processes, Far East Branch Russian Academy of Science, Vladivostok, Russia
[4] The Institute for Physics of Microstructures of the Russian Academy of Sciences, the Federal research center „Institute of Applied Physics named after A. V. Gaponov-Grekhov“, Nizhny Novgorod, Russia

e-mail: batalov@kfti.knc.ru

Received October 02, 2024
Revised October 28, 2024
Accepted October 29, 2024

In this work, in order to obtain highly doped germanium layers with donor impurity of antimony (Ge:Sb), promising for optoelectronic applications, the deposition of 200 nm thick Ge:Sb layers on a single-crystal *p*-Ge substrate was carried out by ion-beam sputtering followed by pulsed ion-beam treatment in the liquid-phase mode. The depth distribution of Sb atoms in Ge before and after pulsed treatment was studied by secondary ion mass spectrometry. The structural state of the Ge:Sb layers was studied by X-ray diffraction and Raman spectroscopy. The optical properties of Ge:Sb layers in the near and mid-IR region ($1-10\,\mu$m) were investigated by measuring the transmission, reflection and photoluminescence at 300 K. The photoresponse of *n*-Ge:Sb/*p*-Ge diode structures was also studied at 300 K. It was found that pulsed ion-beam treatment in the melt mode leads to antimony diffusion into the Ge crystal to $1\,\mu$m, the formation of a single-crystal Ge:Sb layer with a tensile strain of 0.8%, a drop in sample transmittance to zero for $\lambda > 5\,\mu$m, the formation of a high electron concentration in the layer ($1.5 \cdot 10^{20}\,\mathrm{cm}^{-3}$), an enhancement of the direct-band photoluminescence at $\lambda = 1.66\,\mu$m and to obtaining an extended photoresponse to about $\approx 2\,\mu$m.

Keywords: germanium, antimony, doping, ion-beam sputtering, pulsed ion-beam treatment, melting, crystallization, photoluminescence, photoresponse, optoelectronics.

DOI: 10.61011/EOS.2024.11.60320.7119-24

Introduction

Crystalline germanium (Ge) is a narrow-bandgap semiconductor with an indirect band structure because the minimum energy difference between the valence band top at the Γ-point of the Brillouin zone and the conduction band minimum at the *L*-point is $E_g = 0.67\,\mathrm{eV}$ (indirect transition) compared to the energy of 0.8 eV corresponding to the direct transition at the Γ-point [1]. Germanium effectively absorbs visible and near-infrared (IR) light (transmittance $T = 0$ at $\lambda \approx 1.7\,\mu$m) and becomes transparent in the$\lambda = 2-12\,\mu$m range ($T \approx 45\%$) [2]. At the same time, the indirect band structure of Ge prevents an efficient radiative transition, which limits the use of Ge as the active medium of light-emitting diodes and lasers. Therefore, Ge is used in the optical industry as a material for IR photodetectors for the $0.8-1.7\,\mu$m wavelength region and as a material for transmissive IR optics (windows, lenses) for thermography, pyrometry, and spectroscopy.

Since the energy difference between the conduction band minima in the *L*- and Γ-valleys is only 0.13 eV, by reducing this small difference to zero due to external influences, a pseudo-direct-band semiconductor can be obtained. To reduce the energy difference, the introduction of tensile strain of about 0.2% in the epitaxial layers of Ge on the Si substrate due to the difference in the thermal expansion coefficients of the Ge film and the Si substrate, as well as the introduction of donor impurity (P, As, Sb) into Ge with a concentration above $10^{19}\,\mathrm{cm}^{-3}$ to fill the electrons of the direct Γ-valley has been used [3]. Higher values of tensile strain (up to 2%), at which Ge can become a direct band, can be obtained by its epitaxial growth on substrates with a large lattice parameter, such as $Ge_{1-x}Sn_x$ [4] or $In_xGa_{1-x}As$ [5], or by creating membrane (bridging) structures of Ge [6,7].

To date, the metal–oxide–semiconductor field-effect transistors (MOSFET) [8], photodetectors with an extended edge of long-wavelength photosensitivity (up to $1.8\,\mu$m) [6],

light-emitting diodes and lasers with emission wavelength $1.5-1.7\,\mu$m [3,9,10], as well as thin-film chemical sensors [11] have been obtained using strained and heavily doped Ge. In this case, the main methods for the preparation of modified Ge were metalorganic vapour phase epitaxy (MOVPE) or molecular beam (MBE) epitaxy with the introduction of donor impurity (P, Sb) during growth to the level of $3 \cdot 10^{20}\,\mathrm{cm}^{-3}$ [12–14]. Such donor impurity concentration is comparable to the equilibrium solubility for P in Ge ($2 \cdot 10^{20}\,\mathrm{cm}^{-3}$ at 580°C) and an order of magnitude higher than the equilibrium solubility for Sb in Ge ($1.1 \cdot 10^{19}\,\mathrm{cm}^{-3}$ at 800°C) [3]. However, it is difficult by these methods to obtain free electron concentrations above $10^{20}\,\mathrm{cm}^{-3}$, which is required for various optoelectronic and plasmonic applications.

Achieving such high carrier concentrations is possible using strongly non-equilibrium techniques such as ion implantation or pulsed laser annealing (PLA) [15]. We have previously shown that PLA by a ruby laser ($\lambda = 694$ nm, $\tau = 70$ ns) of Ge layers with Sb impurity ($N_{\mathrm{Sb}} \sim 1$ at.%), deposited by ion sputtering on Si, sapphire, and quartz substrates led to effective activation of impurity Sb atoms (almost up to 100%) reaching the maximum electron concentration $5.5 \cdot 10^{20}\,\mathrm{cm}^{-3}$on the quartz substrate according to Hall measurements [16]. It should be noted that the Ge:Sb layers were polycrystalline after PLA. In [17] the PLA of both implanted Ge:Sb^+ layers on *p*-Ge substrate and $Ge_{1-x}Sb_x$ ($x = 0.06$ or $2.5 \cdot 10^{21}$ cm $^{-3}$) deposited by MBE method (at $T = 100$°C) on germanium-on-insulator substrate ($Ge/SiO_2/Si$) was carried out. According to the Rutherford backscattering (RBS) data, annealing of the implanted layers showed a substitutional concentration of Sb atoms in the Ge lattice at the level of $5 \cdot 10^{20}\,\mathrm{cm}^{-3}$ and a higher concentration of $\sim 1.3 \cdot 10^{21}\,\mathrm{cm}^{-3}$ for the deposited samples. In both cases, the Ge:Sb layers after PLA were epitaxial and strained due to the larger ionic radius of Sb compared to Ge.

In [18], the effect of excimer laser ($\lambda = 308$ nm, 28 ns) on 500 nm thick epitaxially grown (at $T = 500$°C) by CVD with phosphorus impurity with $10^{20}\,\mathrm{cm}^{-3}$concentration was investigated. It was shown that as a result of PLA, the tensile strain level increased from 0.05 to 0.37%, the carrier concentration increased from $2 \cdot 10^{19}$ to $9 \cdot 10^{19}\,\mathrm{cm}^{-3}$, and the photoluminescence (PL) spectra at 300 K showed a shift in the main peak at 1670 nm from a direct transition through the Γ-valley to a peak at 1800 nm, while the contribution of the indirect transition through the *L*-valley was strongly reduced.

Also in a recent study [19] the doping of Ge with Sb impurity from a deposited Sb film as a result of UV-PLA ($\lambda = 355$ nm, 7 ns or $\lambda = 248$ nm, 22 ns) was performed. It was shown that the maximum carrier concentration in the Ge:Sb layer after PLA reached $\sim 3 \cdot 10^{20}\,\mathrm{cm}^{-3}$ (plasma wavelength $\lambda_p = 2.6\,\mu$m), and the tensile strain level was 0.57–0.68% depending on the laser type. No PL measurements were performed on Ge:Sb layers.

Pulsed ion-beam treatment (PIBT) with a high-power ion beam of C^+/H^+ composition of nanosecond duration can serve as an alternative to PLA. High-power ion beams are generated at the pulsed ion accelerator TEMP [20,21], and such treatment, similar to PLA, is accompanied by intensive heating of the near-surface region to melting or vaporization. In contrast to PLA, such a treatment does not depend on the optical properties of the material, since all the energy of the ion beam is absorbed in the material and there are no energy losses for reflection. At the same time, the ion beam energy is released more uniformly in the ion projection region (about $1\,\mu$m). We have previously investigated the effect of PIBT on heavily doped Ge:Sb layers obtained by ion implantation [22] and ion sputtering [23,24] methods.

In [24], pulsed heating calculations of the Ge wafer were performed, which showed that at an ion beam energy density of $W = 0.4\,\mathrm{J/cm}^2$ the temperature at the Ge surface exceeds the melting point (940°C), and the melt depth is $0.3\,\mu$m. At $W = 1.0\,\mathrm{J/cm}^2$ the calculated melt depth reaches $1.4\,\mu$m, and the temperature at the surface is 2400°C. Measurements of the depth distribution of Sb in Ge after PIBT showed antimony diffusion in the melt up to $1.4\,\mu$m, which is consistent with the thermal calculations. The study [22] investigated the optical properties of implanted Ge:Sb^+ layers after PIBT, which showed an increase in the direct bandgap contribution to the PL signal at $1.61\,\mu$m compared to the original Ge crystal (peak at $1.79\,\mu$m). In this paper, which is a continuation of the above-mentioned works, the structure, optical and photoelectric properties of Ge layers with higher Sb concentration (~ 1 at.%) obtained on *p*-Ge substrate by ion-beam methods have been investigated.

Experimental procedure

Double-sided polished single crystals of Ge grade GDG-40 with thickness 0.5 mm, *p*-type conductivity with orientation (111) were used as substrates. Deposition of Ge:Sb layers on purified *p*-Ge substrates was carried out by ion-beam sputtering of a composite target ⟨Sb/Ge⟩ by a wide-aperture xenon ion beam (Xe^+) with energy $E = 1.3$ keV at ion current density $j = 150\,\mu\mathrm{A/cm}^2$ during 10 min. Details of the deposition process of the Ge:Sb layer can be found in [16].

To crystallize the deposited layers and to electrically activate the Sb impurity, a PIBT on a TEMP-4M accelerator was used. The parameters of the high-power ion beam were as follows: beam composition $C^+ \sim 80\%$, $H^+ \sim 20\%$, vacuum before the start of the $p \sim 10^{-5}$ Torr, ion energy $E \sim 300$ keV, pulse duration $t \sim 100$ ns, energy density $W \sim 0.8\,\mathrm{J/cm}^2$. The depth distribution of Sb atoms in Ge before and after PIBT was investigated by time-of-flight secondary ion mass spectrometry (ToF-SIMS) on a TOF.SIMS5 (ION-TOF) instrument by layer-by-layer ion etching. The vacuum level in the chamber during the measurements was $p \sim 10^{-10}$ Torr. The surface etching and its analysis were

carried out by synchronous alternation of pulsed ion beams Cs^+ (1 keV, 70 nA) and Bi^+ (25 keV, 1 pA) respectively. Experimentally obtained values of current pulses were converted to the impurity atom concentration scale based on a reference sample obtained by low-dose implantation of Sb^+ ions in Ge. The depth scale was obtained by measuring the depth of the etch pit with a profilometer.

The crystal structure of the deposited and pulse annealed Ge:Sb layers was investigated by glancing angle X-ray diffraction (XRD) on a DRON-7 diffractometer („Burevestnik"). The glancing angle of X-rays (CuK_α radiation) was $\varphi = 1-3°$, which corresponded to the analysis depth up to 1 μm. Also, to evaluate the degree of crystallization and deformation in Ge:Sb layers, Raman spectroscopy (RS) on an NTEGRA SPECTRA spectrometer (NT-MDT) using Ar-laser radiation (488 nm, 0.5 mW) was applied. The optical properties of the obtained samples were investigated for transmission (T) and reflection (R) in the $1-10\,\mu$m wavelength region using a Bruker Vertex 80v IR Fourier spectrometer. From the reflectance spectra, the carrier concentration was estimated from the position of the plasma minimum. Electrophysical measurements of the samples at 300 K were also carried out to determine the layer resistivity and layer carrier concentration.

Photoluminescence of the original p-Ge substrate and Ge:Sb layers was measured at $T = 300$ K using an ACTON 2300i monochromator and a cooled OMA-V photodetector consisting of a linear array of InGaAs-based photodiodes with an operating photosensitivity range of $\lambda = 0.8-2.1\,\mu$m. A continuous infrared laser with a wavelength of 808 nm and a power up to 300 mW was used for PL excitation.

For photoelectric measurements, mesadiode structures of 3×3 mm in size and about 1 μm in height were prepared on the n-Ge:Sb/p-Ge sample by chemical etching in a mixture of hydrofluoric and nitric acids. To evaluate the quality of the diode structure, volt-ampere characteristic (VAC) measurements were performed on a setup assembled from a programmable power supply and current and voltage meters. Photoresponse measurements of the obtained n-Ge:Sb/p-Ge sample and a commercial Ge-photodiode (PD-10GB) were carried out on a setup consisting of an MDR-206 monochromator (LOMO Photonics), a 150 W incandescent lamp, a 500 Hz modulator, and an SDM (LED Microsensor NT) synchronous detection board. The photoresponse was determined as the difference between the analogue-to-digital converter (ADC) counts when the sample was illuminated by the lamp and in the dark.

Results and discussion

The depth distribution of Sb atoms embedded in the Ge layer during ion sputtering and subsequent PIBT was investigated by SIMS method. Figure 1 shows the concentration profiles of Sb atoms in Ge after vacuum deposition (curve *1*, $W = 0$) and after PIBT (curve *2*, $W = 0.8$ J/cm^2). The initial profile of Sb atoms has a shape close to rectangular,

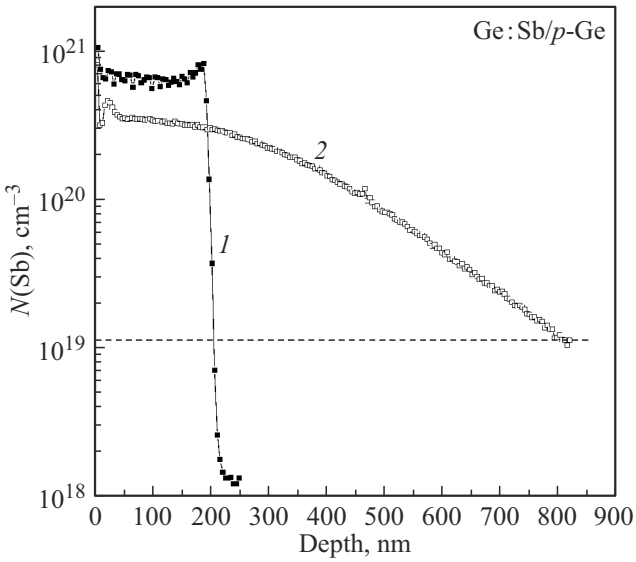

Figure 1. Depth distribution of Sb atoms in Ge obtained by SIMS after ion sputtering (*1*, $W = 0$) and after PIBT (*2*, $W = 0.8$ J/cm^2). The horizontal dashed line — the equilibrium solubility limit of Sb in Ge, equal to $1.1 \cdot 10^{19}$ cm^{-3}.

with a doped Ge:Sb layer thickness of about 200 nm and a maximum concentration of $(6-8) \cdot 10^{20}$ cm^{-3} (sheet layer concentration $1.4 \cdot 10^{16}$ cm^{-2}). This value is well above the equilibrium solubility limit, which is $1.1 \cdot 10^{19}$ cm^{-3} (horizontal dashed line). After PIBT with an energy density of $W = 0.8$ J/cm^2 accompanied, according to the calculations [24] by the formation of a melt with a thickness of $\sim 1.1\,\mu$m, Sb atoms diffuse in the melt to a measured depth of ~ 800 nm at a concentration level of about 10^{19} cm^{-3} forming a profile with changing concentration. Along with diffusion into the Ge crystal depth, a part of Sb atoms is displaced by the crystallization front into the region of increased concentration near the surface (segregation effect), where the Sb concentration is about $4.4 \cdot 10^{20}$ cm^{-3}. A similar Sb segregation peak was observed by us earlier in [16].

To determine the structural state of the Ge:Sb layer after ion sputtering and PIBT, glancing angle X-ray diffraction studies were carried out and the results are shown in Figure 2 for the incidence angle of X-rays $\varphi = 2°$. The lower spectrum (curve *1*) is the spectrum of the original p-Ge(111), substrate, characterized by two weak peaks from the Ge(111) and Ge(400) planes. This spectrum was recorded with less accumulation than the subsequent spectra. The spectrum *2* from the Ge:Sb layer after ion sputtering shows the amorphous structure of the layer, judging by two broad overlapping Ge peaks at angles $2\theta \sim 28°$and $\sim 49°$. The first peak at $2\theta \sim 28°$ is close in position to the Ge(111) peak. Second broad peak at $2\theta \sim 49°$ is the sum of the contributions of the Ge(220), Ge(311), and Ge(222) peaks. The upper spectrum (curve *3*) corresponds to the sample after PIBT with $W = 0.8$ J/cm^2. As can be

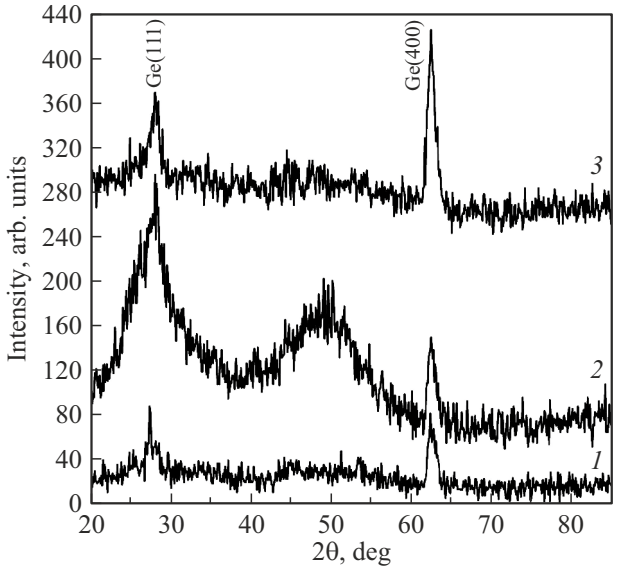

Figure 2. The glancing angle X-ray diffraction spectra (beam incident angle $\varphi = 2^\circ$) of the original *p*-Ge(111) single crystal (spectrum *1*), the Ge:Sb layer after ion sputtering (spectrum *2*), and after PIBT (spectrum *3*). Spectra *2* and *3* are shifted vertically for clarity

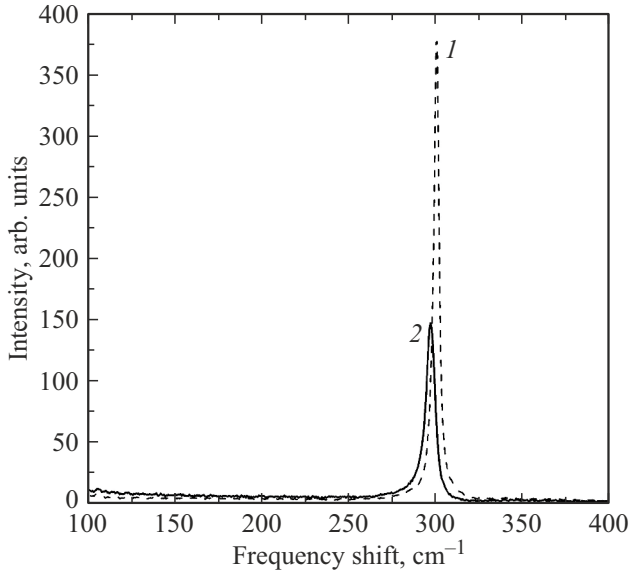

Figure 3. RS spectra obtained from the initial substrate *p*-Ge(111) (*1*) and from the Ge:Sb layer after ion sputtering and PIBT ($W = 0.8\,\mathrm{J/cm^2}$) (*2*).

seen, two peaks identical to the original Ge(111) substrate remain in the spectrum. The absence of amorphous and polycrystalline Ge peaks in the spectrum, as well as the preservation of Sb impurity in the layer (absence of its evaporation) (Fig. 1) indicates the formation of a single-crystal structure of the Ge:Sb layer. The formation of a single-crystalline Ge:Sb layer on the Ge(111) substrate as

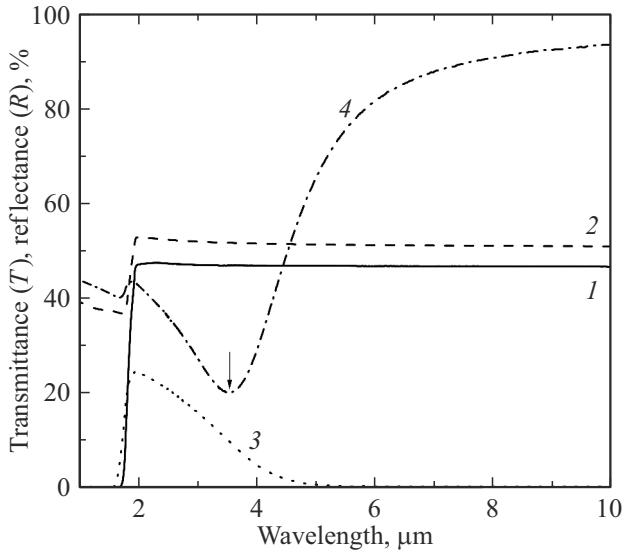

Figure 4. Infrared transmission *T* and reflection *R* spectra of the initial *p*-Ge crystal (respectively *1* and *2*) and Ge:Sb/*p*-Ge sample after PIBT ($W = 0.8\,\mathrm{J/cm^2}$) (respectively *3* and *4*).

a result of PIBT was observed by us earlier in [22–24], including the electron diffraction method.

To further structurally characterise the sample, the RS method was used and its results are shown in Figure 3. This figure shows the spectra of the original *p*-Ge substrate (curve *1*) and the Ge:Sb layer after deposition and PIBT (curve *2*). The spectrum of the *p*-Ge substrate is characterised by an intense symmetric peak at 301.06 cm^{-1} with a half-width of 3.5 cm^{-1}. The spectrum of the Ge:Sb layer obtained by ion sputtering (not shown) is characterised by a broad peak at $\sim 270\,\mathrm{cm^{-1}}$ typical of amorphous Ge. We observed a similar peak on Ge layers deposited on Si, Al_2O_3 and SiO_2 substrates [25]. The spectrum of the pulse annealed Ge:Sb layer is characterised by an asymmetric peak at 297.74 cm^{-1} with a half-width of 6.2 cm^{-1}. The asymmetry of the peak and its increased half-width are probably related to the residual defects in the Ge:Sb layer (vacancies, interstitials, Sb clusters, etc.) after PIBT. Based on the given peak values, the difference between the peak positions is $\Delta\omega = 3.32\,\mathrm{cm^{-1}}$. This difference characterises the tensile-stress state of the heavily doped Ge:Sb layer. Using the formula $\Delta\omega = b\varepsilon$, where $b = -(415 \pm 40)\,\mathrm{cm^{-1}}$ from [26], we can estimate the average level of tensile strain in the layer, which was $\varepsilon = -0.8\%$. This rather large strain can be attributed to the ultrahigh doping level (up to $4.4 \cdot 10^{20}\,\mathrm{cm^{-3}}$) of the Sb impurity and to the thermal stresses in the Ge wafer during the PIBT process caused by the temperature gradient between the highly heated $1-2\,\mu$m thick layer and the relatively cold $500\,\mu$m-thick substrate. It should be noted that at higher values of the ion beam energy density ($W > 1.5\,\mathrm{J/cm^2}$) the cracking of Ge and other semiconductor (Si, GaAs) wafers becomes possible.

Let us next consider the optical measurement data. Figure 4 shows the $T(\lambda)$ transmission and $R(\lambda)$ reflection spectra in the IR region ($\lambda = 1-10\,\mu$m) of the original *p*-Ge single crystal (curves *1* and *2*) and the Ge:Sb/*p*-Ge sample after annealing (curves *3* and *4*). The Ge single crystal is characterised by a sharp increase in transmittance from zero to $\sim 45\%$ in the wavelength region $1.5-2\,\mu$m due to the fundamental absorption edge ($E_g = 0.67$ eV). In the $2-10\,\mu$m wavelength range, the *p*-Ge transmittance is almost unchanged and remains at 46–47%. The *p*-Ge reflectance is also kept constant at $\sim 50\%$ over the $2-10\,\mu$m wavelength range. To compare, sample Ge:Sb/*p*-Ge after PIBT has a less sharp absorption edge and a much lower transmittance level ($T = 25\%$ at $2\,\mu$m), which drops to zero at $\lambda > 5\,\mu$m. This is caused by the strong increase in absorption in the sample due to the ultra-high concentration of embedded antimony ($\sim 4 \cdot 10^{20}\,\mathrm{cm}^{-3}$). The reflection spectrum of the sample is characterised by a distinct minimum in the $3.5\,\mu$m region and a subsequent sharp increase in reflection up to 93% at $\lambda = 10\,\mu$m. This kind of reflection spectrum is typical for highly doped semiconductors, where the concentration of carriers exceeds $10^{19}\,\mathrm{cm}^{-3}$ and is associated with the manifestation of the plasma effect [27]. From the position of the reflection minimum (ω_p) the integral concentration of charge carriers (electrons) in the Ge:Sb layer can be estimated in a non-contact manner using a formula that takes into account the charge e and the effective mass m^* of the electron, as well as the dielectric constant ε of germanium: $N_e = \omega_p^2 \frac{10^{18}}{A^2}$, where the parameter $A = 2.85 \cdot 10^{-2}$ eV. For the value $\omega_p = 0.35$ eV ($\lambda = 3.5\,\mu$m) the electron concentration is $1.5 \cdot 10^{20}\,\mathrm{cm}^{-3}$. Since the maximum concentration of Sb atoms near the surface after PIBT is $4.4 \cdot 10^{20}\,\mathrm{cm}^{-3}$ (Fig. 1), it turns out that only one third of Sb atoms near the surface are electrically active. The rest of the Sb atoms are probably located either in the interstitial positions of the Ge crystal lattice or in the form of clusters. It should be borne in mind that the degree of activation of the impurity increases with the decrease of its concentration in the depth of the sample (for thicknesses exceeding ~ 500 nm), where the activation can be complete, i.e. there is a coincidence of the concentration of the impurity and electrons.

We also carried out electrophysical measurements of the n^+-Ge:Sb/*p*-Ge sample in van der Pauw geometry to determine the sheet resistance of R_s and the layer carrier concentration N_s. DC measurements of 0.5 mA gave $R_s = 4.5\,\Omega/\square$, and Hall measurements in a magnetic field of 0.34 T produced $N_s = 9 \cdot 10^{15}\,\mathrm{cm}^{-2}$. In this case, the determination of resistivity and bulk carrier concentration is complicated by the choice of a suitable layer thickness due to the variation of impurity concentration with depth.

The optical properties of the n^+-Ge:Sb/*p*-Ge sample after PIBT were also investigated by the PL method at $T = 300$ K and under pumping by a continuous IR laser ($\lambda = 808$ nm) with a power of 300 mW (Fig. 5, curve *2*). The PL spectrum of the original *p*-Ge substrate (curve *1*) is also shown there for comparison. The spectrum of the initial *p*-Ge crystal is characterised by a broad band with a maximum at $1.77\,\mu$m (0.7 eV). The position of the maximum is close to the bandgap of bulk Ge (0.67 eV) and is due to the optical transition from the indirect *L*-valley. At the same time, the contribution from the direct transition from the Γ-valley at $1.55\,\mu$m (0.8 eV) is indistinguishable.

At the same time, the PL spectrum of the n^+-Ge:Sb/*p*-Ge, sample obtained by ion sputtering and PIBT methods is characterised by an intense maximum at $1.66\,\mu$m (0.747 eV), a weak „arm“ on the right side at $2\,\mu$m (0.615 eV) and a „ledge“ on the left side at $\sim 1.3\,\mu$m (0.96 eV). Since strong doping and tensile strain lead to narrowing of the gaps in the *L*- and Γ-valleys [3], we can assume that the „shoulder“ on the right is due to the optical transition through the indirect *L*-valley, the energy of which decreased from 0.7 to 0.615 eV. The main maximum is due to the optical transition through the direct Γ-valley, whose energy decreased from 0.8 to 0.747 eV, and the „ledge“ on the left is due to the optical transitions through the indirect *X*-valley — in accordance with the energy band diagram and experimental data on laser annealing of implanted Ge from [28]. Thus, the high degree of tensile strain ($\varepsilon = -0.8\%$), caused by ultrahigh concentration of Sb impurity ($N_{\mathrm{Sb}} = 4.4 \cdot 10^{20}\,\mathrm{cm}^{-3}$) and thermal stresses induced as a result of PIBT leads to the pseudo-direct-bandgap semiconductor with intense luminescence at room temperature.

Since the obtained sample had a heavily doped n^+-Ge:Sb layer on an *p*-Ge substrate, i.e., it had a diode structure, VAC measurements were carried out to evaluate its quality. The measurement results showed that in the voltage range of ± 4 V the reverse current is 0.5 mA, and the forward current reaches 62.5 mA. The results of the spectral dependence of

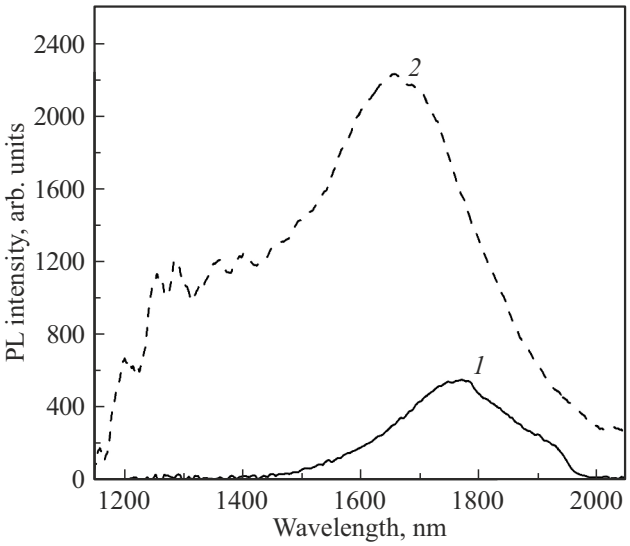

Figure 5. IR PL spectra measured at room temperature, from the original *p*-Ge (*1*) substrate and the Ge:Sb (*2*) layer, when pumped by an IR laser with a wavelength of 808 nm and a power of 300 mW.

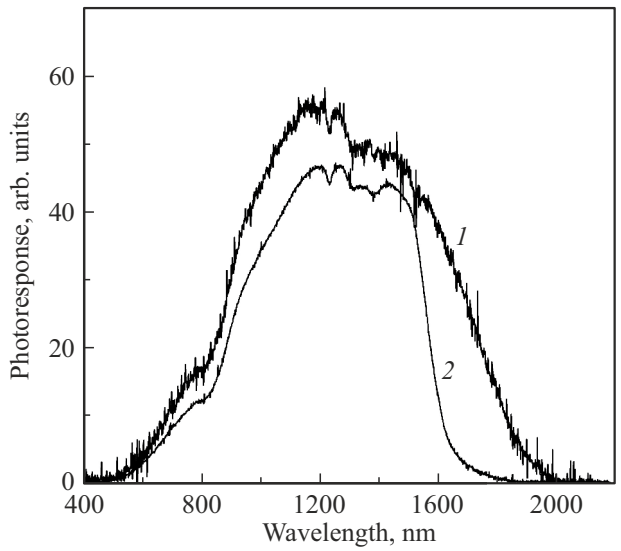

Figure 6. Spectral dependence of the photo-response in visible and IR regions taken at room temperature for the mesadiode structure n^+-Ge:Sb/p-Ge (*1*) and for the commercial Ge-photodiode FD-10GB (*2*) at reverse voltage $U = 8$ V.

the photoresponse of the n^+-Ge:Sb/p-Ge sample (curve *1*) and the commercial Ge-photodiode FD-10GB (curve *2*) when the reverse voltage $U = 8$ V is applied are shown in Figure 6. It can be seen that the sample signal has a larger area under the curve, a smoother decline in the long-wavelength region, and a photoresponse extended to $2\,\mu$m. The higher noise level in the spectrum of the sample is due to the clamping electrical contacts to the Ge:Sb layer. The probable reason for the extension of the long-wavelength limit of the photosensitivity of the sample is the narrowing of the bandgap of Ge due to the strong doping of the Ge:Sb layer and its stretching.

Conclusion

Achieving high levels of Ge doping with donor impurities is currently an urgent problem in micro- and optoelectronics. In this study, Ge:Sb layers were deposited on a single-crystal p-Ge substrate by ion sputtering of a composite target with a high-current xenon ion beam. The thickness of the deposited layers was 200 nm, and the antimony impurity concentration — to $8 \cdot 10^{20}\,\mathrm{cm}^{-3}$. Melt mode PIBT was used for crystallization of the layers and electrical activation of impurity atoms. SIMS, XRD, RS, PL, as well as transmission, reflection and photo-response measurements were used to investigate the structural and optical properties of heavily doped Ge:Sb layers. The formation of tensile-strained single-crystalline Ge:Sb layer with thickness up to $1\,\mu$m with maximum antimony concentration near the surface $4.4 \cdot 10^{20}\,\mathrm{cm}^{-3}$ was found. Only one third of this concentration of antimony atoms near the surface is electrically active. The high integrated carrier concentration in the layer ($1.5 \cdot 10^{20}\,\mathrm{cm}^{-3}$) estimated from the reflection spectrum, leads to a drop in the transmittance in the sample to zero for $\lambda > 5\,\mu$m, enhanced direct-band PL ($\lambda = 1.66\,\mu$m at 300 K) and enhanced photoresponse (up to $\lambda = 2\,\mu$m). The results of this work can be used for the development of LEDs and photodiodes based on germanium.

Funding

The study was performed within the framework of the State Order (Ministry of Science and Higher Education of the Russian Federation) of E.K. Zavoysky Kazan Physical-Technical Institute of the Federal Research Centre „Kazan Scientific Centre of the Russian Academy of Sciences“.

Conflict of interest

The authors declare that they have no conflict of interest.

References

[1] *NSM Archive — Physical Properties of Semiconductors* [Electronic resource]. URL: http://www.matprop.ru/Ge_bandstr
[2] Tydex. Materials for transmission optics (*germanium*) [Electronic resource]. URL: https://www.tydexoptics.com/ru/materials/for_transmission_optics/germanium/
[3] J. Liu, L.C. Kimerling, J. Michel. Semicond. Sci. Technol., **27**, 094006 (2012). DOI: 10.1088/0268-1242/27/9/094006
[4] S. Takeuchi, Y. Shimura, O. Nakatsuka, S. Zaima, M. Ogawa, A. Sakai. Appl. Phys. Lett., **92**, 231916 (2008). DOI:10.1063/1.2945629
[5] Y. Bai, K.E. Lee, C. Cheng, M.L. Lee, E.A. Fitzgerald. J. Appl. Phys., **104**, 084518 (2008). DOI:10.1063/1.3005886
[6] D. Nam, D. Sukhdeo, A. Roy, K. Balram, S.-L. Cheng, K.C.-Y. Huang, Z. Yuan, M. Brongersma, Y. Nishi, D. Miller, K. Saraswat. Optics Express, **19** (27), 25866 (2011). DOI: 10.1364/OE.19.025866
[7] N.A. Baidakova, A.N. Yablonsky, N.S. Gusev, K.E. Kudryavtsev, E.E. Morozova, D.V. Yurasov, V.Ya. Aleshkin, A.V. Nezhdanov, A.V. Novikov. FTP, **56** (10), 954 (2022). (in Russian) DOI: 10.21883/FTP.2022.10.53955.9852
[8] R. Pillarisetty. Nature, **479**, 324 (2011). DOI: 10.1038/nature10678
[9] S. Saito, A.Z. Al-Attili, K. Oda, Y. Ishikawa. Semicond. Sci. Technol., **31**, 043002 (2016). DOI: 10.1088/0268-1242/31/4/043002
[10] A.M. Titova, V.G. Shengurov, D.O. Filatov, S.A. Denisov, V.Yu. Chalkov, M.V. Ved', A.V. Zaitzev, A.A. Sushkov, N.A. Alyabina. Mater. Sci. Eng. B, **289**, 116219 (2023). DOI: 10.1016/j.mseb.2022.116219
[11] L. Baldassarre, E. Sakat, J. Frigerio, A. Samarelli, K. Gallacher, E. Calandrini, G. Isella, D.J. Paul, M. Ortolani, P. Biagioni. Nano Lett., **15**, 7225 (2015). DOI: 10.1021/acs.nanolett.5b03247
[12] J.M. Hartmann, J.P. Barnes, M. Veillerot, J.M. Fedeli, Q. Benoit A La Guillaume, V. Calvo. J. Cryst. Growth, **347**, 37 (2012). DOI: 10.1016/j.jcrysgro.2012.03.023

[13] D.V. Yurasov, A.V. Antonov, M.N. Drozdov, P.A. Yunin, B.A. Andreev, P.A. Bushuykin, N.A. Baydakova, A.V. Novikov. J. Cryst. Growth, **491**, 26 (2018). DOI: /10.1016/j.jcrysgro.2018.03.037
[14] D.S. Prokhorov, V.G. Shengurov, S.A. Denisov, D.O. Filatov, A.V. Zdoroveyshchev, V.Y. Chalkov, A.V. Zaitsev, M.V. Ved, M.V. Dorokhin, N.A. Baidakova. Semicnd., **53** (9), 1293 (2019). (in Russian) DOI: 10.21883/FTP.2019.09.48142.26
[15] A.V. Dvurechensky, G.A. Kachurin, E.V. Nidaev, L.S. Smirnov. *Impulsny otzhig poluprovodnikovykh materialov* (Nauka, M., 1982).
[16] R.I. Batalov, R.M. Bayazitov, I.A. Faizrakhmanov, N.M. Lyadov, V.A. Shustov, G.D. Ivlev. J. Phys. D, **49**, 395102 (2016). DOI: 10.1088/0022-3727/49/39/395102
[17] E. Bruno, G.G. Scapellato, G. Bisognin, E. Carria, L. Romano, A. Carnera, F. Priolo. J. Appl. Phys., **108**, 124902 (2010). DOI: 10.1063/1.3520671
[18] J. Frigerio, A. Balladio, K. Gallacher, V. Gilberti, L. Baldassarre, R. Millar, R. Milazzo, L. Maiolo, A. Minotti, F. Bottegoni, P. Biagioni, D. Paul, M. Ortolani, A. Pecora, E. Napollitani, G. Isella. J. Phys. D, **50**, 465103 (2017). DOI: 10.1088/1361-6463/aa8eca
[19] C. Carraro, R. Milazzo, F. Sgarbossa, D. Fontana, G. Maggioni, W. Raniero, D. Scarpa, L. Baldassarre, M. Ortolani, A. Andrighetto, D.R. Napoli, D. De Salvador, E. Napolitani. Appl. Surf. Sci., **509**, 145229 (2020). DOI: 10.1016/j.apsusc.2019.145229
[20] G.E. Remnev, I.F. Isakov, M.S. Opekounov, G.I. Kotlyarevsky, V.L. Kutuzov, V.S. Lopatin, V.M. Matvienko, M.Yu. Ovsyannikov, A.V. Potyomkin, V.A. Tarbokov. Surf. Coat. Technol., **96**, 103 (1997). DOI: 10.1016/S0257-8972(97)00116-3
[21] A.I. Pushkarev, Y.I. Egorova, A.I. Prima, P.M. Korusenko, S.N. Nesov. *Generatsyya, diagnostika i primenenie moschnykh ion'nykh puchkov s vysokoy plotnostiyu energii* (ANS „SibAC", Novosibirsk, 2019).
[22] R.I. Batalov, R.M. Bayazitov, G.A. Novikov, V.A. Shustov, N.M. Lyadov, A.V. Novikov, P.A. Bushuikin, N.A. Baidakova, M.N. Drozdov, P.A. Yunin. Avtometriya. **55**, 5 (2019). (in Russian). DOI: 10.15372/AUT20190501
[23] R.M. Bayazitov, R.I. Batalov, G.A. Novikov, I.A. Fayzrakhmanov, N.M. Lyadov, V.A. Shustov, V.V. Vorobyev. Ezhegodnik KFTI 2016, 80–85 (2017). (in Russian)
[24] R.I. Batalov, R.M. Bayazitov, G.A. Novikov, I.A. Fayzrakhmanov, V.A. Shustov, G.D. Ivlev. Mikroelektronika, **47** (74), (2018) (in Russian). DOI: 10.31857/S054412690001740-1
[25] G.A. Novikov, R.I. Batalov, R.M. Bayazitov, I.A. Fayzrakhmanov, N.M. Lyadov, V.A. Shustov, K.N. Galkin, N.G. Galkin, I.M. Chernev, G.D. Ivlevlev, S.L. Prokopyev, P.I. Gaiduk. FTP, **49** (6), 746 (2015). (in Russian)
[26] Y.-Y. Fang, J. Tolle, R. Roucka, A.V.G. Chizmeshya, J. Kouvetakis, V.R. D'Costa, J. Menendez. Appl. Phys. Lett., **90**, 061915 (2007). DOI: 10.1063/1.2472273
[27] J. Pankov. *Opticheskie protsesy v poluprovodnikakh* (Mir, M., 1973). (in Russian)
[28] J. Wagner, G. Contreras, A. Compaan, M. Cardona, A. Axmann. Mater. Res. Soc. Symp. Proc., **23**, 147–152 (1984).

Translated by J.Savelyeva